

Supporting Information

Cornforth et al. 10.1073/pnas.1319175111

SI Text

Bacteria are increasingly recognized to be highly social organisms, at times working together to perform impressive feats of collective foraging, defense, or dispersal, mediated by the production of secreted exoproducts such as digestive enzymes, antibiotics, or surfactants (1, 2). Even more impressively, bacteria commonly display complex regulatory control over these secreted factors so that, when conditions are favorable for the population to exert effective control over the local environment, individuals within the population up-regulate a suite of genes, turning on their collective phenotypes (3).

A major strand in the study of bacterial social life has argued that bacteria are able to sense and respond to changes in local densities via a process called “quorum sensing.” Quorum-sensing bacteria produce small diffusible signal molecules, and when the density of these molecules is sufficiently high, the bacteria shift their gene expression. Quorum sensing is now seen to be profoundly important to bacterial behavior, regulating many bacterial genes in various organisms, including those involved in bacterial swarming as well as biofilm and toxin production (Table S2). This great importance has brought quorum sensing intense attention since its discovery. Detailed biochemical pathways for the production, uptake, and regulation of quorum-sensing molecules are available; the signal–receptor interactions are well understood; and, already, biomedical therapies are being developed to disrupt quorum-sensing mechanisms in pathogens within human hosts.

Despite the intense mechanistic scrutiny quorum sensing has received in recent years, there is disagreement about the functional significance of the behavior in bacteria (4–7). The classical interpretation has been that quorum sensing is a proxy for bacterial cell density: the higher the signal concentration, the higher the bacterial density. However, factors other than bacterial density are likely to modify the concentration of bacterially derived molecules (diffusion, degradation, flow, etc.), and, therefore, the resultant changes in gene expression may be more closely tied to changes in physical rather than social variation. Some have argued that, rather than quorum sensing acting to survey cellular density, the information most important for the microbe is abiotic environmental properties (4). When most molecules secreted are lost by mass transfer in the environment, secreting costly molecules makes little sense; so, in effect, these signal molecules may play a role as cheap probes to survey whether more costly secretions are worth producing or would instead be immediately lost. The controversy between classical quorum-sensing interpretations and diffusion-sensing ones remains because, in their starkest forms, both cannot be correct; high autoinducer quantities signify either high bacterial density or low diffusion rate (Fig. 1 and Fig. S1).

It has been argued that this distinction between social and nonsocial influences on signal concentration is unimportant (5); the observation of a moderate or high level of signal molecule should favor the production of more costly secreted factors, regardless of whether the focal cell is able to transform a confined environment alone (a low-density, low-mass transfer environment) or whether it can rely on complementation from multiple neighbors (a high-density, high-mass transfer environment). However, in some cases, this paradigm clearly breaks down. Luminescence in *Vibrio fischeri*, for instance, is not susceptible to mass-transfer properties of the environment, and so the extent of confinement or diffusion is largely immaterial to the investment decision, whereas density is decisive. Mass transfer is probably

also unimportant for pathogens that infect using a contact-based type-3 secretory system because, here, accumulation of the chemical in the environment is unnecessary (8). The existence of down-regulated phenotypes also demonstrates that sometimes phenotypes are down-regulated even as signal density is increased (9). Perhaps most generally, the molecular properties of signal molecules and public-goods molecules are very distinct from one another; not only do signal molecules have different molecular weights and diffusion constants, but, as we will soon show, when secretions interact with the environment to produce a public good, the correspondence between signal density and public-good density can quickly break down.

Bacteria responding to signal densities are operating under conditions of imperfect information and have thus elaborated various heuristics or “rules of thumb” to arrive at robust estimates of the most relevant characteristics of their shared external environment. We illustrate that the use of multiple signals, a practice very common in many well-studied bacteria (Table S2), can give significantly more information than using one molecule alone. In particular, if these signal molecules have differing chemical properties, this can allow bacteria to distinguish between a range of distinct environmental scenarios, including a separation of the effects of bacterial density and environmental properties like diffusion and advection (flow).

The Difficulty: Mass Transfer or Density

The most basic ingredient of quorum-sensing logic is that the density of a signal molecule is reliably informative of the density of bacteria, at least up to the threshold density at which the regulatory shift occurs. Above this point, autoinduction of the signal molecule is well-understood to decouple signal and bacterial density. Fig. 1A illustrates the basic argument schematically. With one signal molecule and a predictable mass-transfer regime (i.e., a known value of m), postautoinduction signal concentration is informative of bacterial density N (i.e., classic quorum sensing). However, it is also true that, for the same signal molecule and a predictable density (i.e., a known value of N), signal concentration is also informative of the mass-transfer regime (diffusion sensing). For bacteria experiencing uncertainty over both N and m , estimates of either parameter are confounded by uncertainty over the other, so that high-density, high-mass transfer environments can be indistinguishable from low-density, low-mass transfer environments.

Two Signals

With two molecules of different durabilities, it is possible for a cell to separate the confounding effects of mass transfer and population density and simultaneously improve resolution of both dimensions (Fig. 1B). In the simplest case, suppose a cell produces molecules of differing durabilities, meaning they naturally break apart at different rates. If, in the cell’s environment, the durable molecule is much more common than the fragile one (compared with their relative rates of production), the relative abundance of the durable molecule indicates there has been little mass-transfer removal of either molecule because the fragile molecules have been around long enough in the local environment to naturally degrade. Conversely, if the two molecules exist in concentrations proportional to their rates of production, then mass transfer must be sufficiently high to mask the differences in their rates of chemical decay. In a sense, the decay of the fragile molecule works as a clock that informs how long typical molecules stay near the cell before diffusing or being

washed away. This concept is illustrated in Fig. S1; in this figure, the four environmental scenarios each display a unique signature in a two-signal language but suffer from ambiguity when only one signal is used.

Analytical Models

We will consider very simple models for the extracellular dynamics of signal and public-goods concentrations (Fig. S2). In our models, secreted molecules are lost by two factors: decay of the molecules themselves at rates specific to each secreted molecule, and mass transfer, which is when the environment washes away the molecules and is the same for all secretions. In our model of signal density, the local density of signal (S) is increased by the production (at baseline per-capita rate p) of signal by local bacteria (at density N) and is decreased by mass transfer (advection at rate m ; independent of molecular design) and by physical decay (at rate u ; sensitive to molecular design). Autoinduction is represented by aS , which is the rate of increased signal induction dependent on present signal concentration. The dynamics of two distinct signal molecules is given by the equations:

$$\frac{dS_1}{dt} = (p + a_1 S_1)N - (m + u_1)S_1$$

$$\frac{dS_2}{dt} = (p + a_2 S_2)N - (m + u_2)S_2.$$

For each, the equilibrium is given by $S_k^* = Np / (m - a_k N + u_k)$. At sufficiently low-density and/or high-mass transfer regimes, the equilibrium is stable (when $Na_k < m + u_k$), and we consider the autoinduction process to be “off.” In contrast, when $Na_k > m + u_k$, the equilibrium becomes unstable (leading to an unconfined increase in S_k), and we consider autoinduction to be “on.”

We can describe public-goods dynamics in a similar manner. We will consider two cases. In the most general scenario, we assume that a secreted molecule of concentration X interacts with the environment to form a beneficial, shared extracellular product of concentration Y . For instance, siderophores bind to iron and can then be imported by bacteria, and proteases break down a protein into usable amino acids. This “two-stage” public-goods scenario, where the secreted product catalyzes the formation of an external and beneficial molecule, can be modeled by the production of a secreted catalyst X at rate P , with decay rate f , driving the production of the beneficial molecule Y , formed when the catalyst molecules interact with another molecule in the environment (we assume this conversion to the beneficial molecule occurs at rate q , proportional to the catalyst concentration). The beneficial molecule Y is consumed at rate c and decays at rate e .

$$\frac{dX}{dt} = PN - (m + f)X$$

$$\frac{dY}{dt} = qX - (cN + m + e)Y.$$

These equations yield the equilibria:

$$X^* = \frac{NP}{m + f}$$

$$Y^* = \frac{PqN}{(m + f)(cN + m + e)}.$$

In our second, and seemingly less-common scenario, the secreted factor generates a benefit that is not susceptible to processes of re-

moval or decay, for example, in cases where the shared benefit is tied to host death or changes in the host immune system. We approach these scenarios by assuming that the benefit of the secreted factor is tied directly to its abundance so that the secreted factor is itself the beneficial product Y :

$$\frac{dY}{dt} = PN - (cN + m + e)Y,$$

yielding the equilibrium $Y^* = PN / (cN + m + e)$.

Fig. S8 illustrates the behavior of a multisignal model as a function of changing density N and mass transfer m for the two-stage and one-stage public-goods scenarios. The parameters in Fig. S8A are the same as in Figs. 1 and 4. Qualitatively, the difference between the two- and one-stage models is that, in the one-stage model, the threshold curve above which production is favored, is linear and well-approximated with a single signal molecule. On the other hand, for the two-stage case, the curve curves upward, which can make the optimal region difficult to approximate with one signal molecule alone and can be better approximated using a combination of the two molecules (using AND-gate signal integration). We show below that, when public goods are of the two-stage type, the contour of equilibrium public good at any threshold level has positive concavity. Because two-stage public goods seem much more abundant, we expect an increased prevalence of AND-gates among secreted factors, which we test in our microarray analysis. However, it is worth noting that being able to separate the {density, mass-transfer} plane into four quadrants can have other functional benefits as well. For instance, some genes may be most advantageous in the environments with highest mass-transfer properties, and either with or without high densities; further detailed study of mappings between environment and gene expression are necessary to further understand these issues.

We can demonstrate that in the two-stage model, the contour of public goods equilibrium at threshold value k has positive concavity as follows: Anytime there is a positive level of public goods at equilibrium, we know $Y^* = \frac{qX^*}{cN + m + e}$, and therefore $qX^* > Y^*cN$. At the threshold $Y^* = k$, we know that $qX^* > kcN$. This means $Pq > ck(m + f)$. Let Z be the value of N such that $Y^* = k$. Then $\frac{d^2Z}{dm^2} = -\frac{2kPq(c(e-f)k + Pq)}{(c(m+f)k - Pq)^3} > 0$. This means that the threshold function has positive concavity for $m \geq 0$. Note that this same argument holds also in the case where the secreted enzyme is degraded in the reaction that produces the beneficial product [such as $dX/dt = PN - (m + f + q)X$].

Simulation Models

To provide an evolutionary exploration of our analytical model, we developed an agent-based model, implemented with a genetic algorithm (Fig. 2A). We considered a population of 1,000 strains, which interacted in clonal groups in environments with varying cellular density and mass-transfer regimes. We defined the environments as a 10×10 grid (100 environments in total), with cellular density varying between $10^{1.5}$ and 10^5 cells per μL , and mass-transfer rate varying between 1.5×10^{-7} and 1.5×10^{-4} $\mu\text{L/s}$. We defined four regulons with different target environmental types for their expression (Fig. 2A):

- i) high-density, low-mass transfer regulon (to be expressed at above median density and below median mass transfer);
- ii) high-density, high-mass transfer regulon (to be expressed at above median density and above median mass transfer);
- iii) low-density, low-mass transfer regulon (to be expressed at below median density and below median mass transfer); and
- iv) low-density, high-mass transfer regulon (to be expressed at below median density and above median mass transfer).

Strains received a payoff B when a regulon was turned on in an appropriate environment and paid a payoff cost C for gene expression whenever a regulon was turned on (regardless of the environment). We used the parameter values $B = 1.5$ and $C = 0.5$ so that correct expression yields a net payoff of 1.

Signal dynamics operated according to the equation $dS_i/dt = (p + a_i S_i)N - (m + u_i)S_i$, where S_i is the concentration of signal, N is the cellular density, p_i is the constitutive rate of signal production, a_i controls the strength of autoinduction, u_i is the signal decay rate, and m is the rate of signal removal by mass transfer. Autoinduction occurs whenever $a_i N > u_i + m$ because, when this condition is satisfied, signal concentration tends toward infinity. The parameters a_i and u_i evolved with mutation in our simulations. Autoinduction parameters were allowed to vary between 10^{-10} and 10^{-4} , and signal-decay rates were allowed to vary between 10^{-11} and 10. The state of each signal (1, autoinduced; 0, not autoinduced) acted as inputs for the following logic gates to determine gene expression:

- i) An AND gate (express only when both signals autoinduced) for the high-density, low-mass transfer regulon.
- ii) An X-durable gate (express when only the durable signal is autoinduced) for the low-density, low-mass transfer regulon.
- iii) An X-fragile gate (express when only the fragile signal is autoinduced) for the high-density, high-mass transfer regulon.
- iv) A NOR gate (express only when no signals are autoinduced) for the low-density, high-mass transfer regulon.

These logic gates were set a priori as they achieve optimal division of the environment, and there are 65,536 possible combinations of logic gates for four regulons, which is too large a phenotypic space to explore in our algorithm.

Our genetic algorithm operates as follows:

- i) An initial population of 1,000 strains was constructed. Decay rates and autoinduction parameters for both signals were set to 10^{-6} and 10^{-7} , respectively.
- ii) Each strain's gene expression patterns were assessed in the 100 possible environments, and fitness payoffs based on these expression patterns were calculated.
- iii) Strains were selected with replacement to reproduce with probability proportional to their relative payoffs (i.e., roulette-wheel selection) to produce a new population of 1,000 strains.
- iv) Strains selected to reproduce underwent mutation with probability 0.01 for all traits. Autoinduction parameters and signal-decay rates had a mutational effect drawn from a normal distribution of mean 0 and SD equal to 1/5 of the range of their possible values. All mutation occurred on the \log_{10} scale for all parameters.
- v) The algorithm returned to step 2 until 3,000 generations were reached.

In total, we performed 100 replicates of our genetic algorithm. To give a baseline for the performance of two-signal systems, we compared their payoffs to the maximum payoff possible using one signal. As one signal can at best dissect the environmental space into two equal parts, the maximum mean payoff for a one-signal network is 0.5.

PAO-JG1 Strain Construction

We constructed a double mutant in the two *N*-Acyl homoserine lactone (AHL) synthase genes, *lasI* and *rhII*, starting with the single mutant in only the *lasI* gene (PAO1 $\Delta lasI$) (10). The approach used was to interrupt the *rhII* gene with a tetracycline (Tc) resistance cassette in the following way. We first conjugated the plasmid pRIC380 $\Delta rhII$ (11) from an *Escherichia coli* donor strain S17-1 into the recipient *lasI* single mutant PAO1 $\Delta lasI$. Conjugation was performed by drying a liquid spot on agar of a 1:1 mix of concentrated donor and recipient cultures and in-

cubating at 30 °C for 6 h. Transconjugants were selected for on pseudomonas isolation agar (Difco) containing 200 $\mu\text{g}\cdot\text{ml}^{-1}$ Tc to obtain single crossover events. To select for double crossover events, a random sample of the resulting transconjugants was grown in 5% salt-free sucrose selection broth medium for 16 h and plated onto 5% salt-free sucrose agar. The colonies growing on sucrose were grid-plated onto carbenicillin 400 $\mu\text{g}\cdot\text{ml}^{-1}$ and gentamicin 100 $\mu\text{g}\cdot\text{ml}^{-1}$. Colonies growing on gentamicin but not on carbenicillin were taken to contain the insertion but not the remainder of the plasmid, thus being double crossover mutants. The *rhII* mutation was confirmed by PCR of the entire region to detect a larger fragment where a successful insertion event had happened in candidate mutants using the parent PAO1 $\Delta lasI$. A single colony of the new mutant was grown in LB containing 200 $\mu\text{g}\cdot\text{ml}^{-1}$ Tc, and a sample of the culture stored at -80 °C in 25% glycerol.

Signal Half-Life Experiments

Synthetic AHLs (chemically identical to their natural counterparts, obtained from the S.P.D. laboratory) were diluted in 1 mL of medium (M9, LB, KB, and BHI) from MeOH stocks (2 mM and 200 μM) to a final concentration of 0.1 μM and 0.01 μM (C4 HSL and 3-oxo-C12 HSL), respectively, at varying intervals. After incubation at 37 °C, the AHL solutions were removed from the incubator and mixed 1:1 with a washed log-phase culture of the appropriate biosensor strain at a density of OD600 0.1 (pSB536 and pSB1075 for C4-HSL and 3-oxo-C12 HSL, respectively) in a microplate. OD600 and luminescence (relative light units, RLU) was measured after 30 min incubation at 37 °C. Luminescence per cell was calculated as RLU/OD600 and compared with a calibration curve (Fig. S5) of known 2 \times serially diluted concentrations to determine AHL concentrations. Decay rates were determined by fitting log-linear models to AHL concentrations over time (Fig. S4). The media constituents were as follows. BHI: (calf brains (infusion from 200 g) 12.5 g/L, beef heart (infusion from 250 g) 5 g/L, peptone 10 g/L, sodium chloride 5 g/L, D(+)-glucose 2 g/L, disodium hydrogen phosphate 2.5 g/L). KB: (protease peptone 20 g/L, dipotassium hydrogen phosphate 1.5 g/L, magnesium sulphate heptahydrate 1.5 g/L, glycerol 10 mL). LB: (tryptone 10 g/L, yeast extract 5 g/L, sodium chloride 10 g/L). M9: (Na₂HPO₄ 6.8 g/L, KH₂PO₄ 3 g/L, NaCl 0.5 g/L, NH₄Cl 0.53 g/L, CaCl₂ 0.0011 g/L, MgSO₄·7H₂O 2.64 g/L).

Microarray Experiment

A double QS synthase mutant of *Pseudomonas aeruginosa* PAO1 *lasI/rhII* (see *PAO-JG1 Strain Construction*) was grown at 37 °C in 25 mL of LB broth and 250-mL flasks with shaking at 200 rpm (approximately 2.2 \times g). Where required, LB broth was supplemented with 15 μM QS signal(s) in the following four treatments: (i) no addition; (ii) *N*-(3-oxododecanoyl)-L-homoserine lactone (3-oxo-C12-HSL); (iii) *N*-butyryl-homoserine lactone (C4-HSL); and (iv) both 3-oxo-C12-HSL and C4-HSL. Two replicate cultures were used for each treatment. RNA was extracted from each culture after 8 h incubation (late exponential/early stationary phase of growth). Cells were treated with RNAprotect Bacteria Reagent (Qiagen), and total RNA extraction was performed with the RNeasy Midi Kit (Qiagen) as per the manufacturer's instructions. For the expression profiling experiments, the microarrays were designed to contain multiple oligonucleotide probes for all of the PAO1 genes, including the small RNA genes, and were purchased from Oxford Gene Technology. For each array, 10 mg of RNA was reverse-transcribed and directly labeled with Cy5-dCTP, and 2 mg of genomic DNA was directly labeled with Cy3-dCTP. Samples were hybridized onto the arrays for 16 h. Scanning of the arrays was performed using the Axon 4000B GenePix Scanner, and the data-extraction software used was GenePix Pro-6, both from Molecular Devices.

For each strain, microarray experiments were performed in duplicate, and data capture was performed using GeneSpring GX10 (Agilent Technologies). Further data analysis was performed using the linear models for microarray data (“limma”) package on the open source statistical platform R (v2.14.2). Following Quantile normalization, differential expression was identified using Bayesian-adjusted t statistics, with false discovery rate correction for multiple testing. In all comparisons, the criterion for differential expression was a false discovery rate-corrected P value of less than 0.05.

Bioinformatic Analysis

The genes in which differential expression was observed were then clustered by expression pattern across the four treatments using k -means clustering of mean standardized expression values (Fig. S7). The most likely number of clusters was determined using the Bayesian information criterion (BIC), which is calculated as

$$\text{BIC} = n * \ln(\sigma_e^2/n) + k * \ln(n),$$

where n is the number of genes clustered, k is the number of parameters fitted ($4 \times$ the number of clusters), and σ_e^2 is the total within-cluster error deviance. The number of clusters with the lowest BIC value is taken as the most likely model (Fig. S6). The relative likelihood of any model i can then be taken as $R_i = \exp[(\text{BIC}_{\min} - \text{BIC}_i)/2]$, where BIC_{\min} is the BIC of the best model

(most likely number of clusters). The likelihood that any model is the best from the model set can then be calculated as $L_i = R_i/\sum_j R_j$. From these likelihoods, we calculated the 95% credible interval of the number of expression clusters present in the dataset.

We used a linear model to test our prediction that the secretome is under synergistic control. The secretome (Fig. S7) was identified using predictions from PSORTb v3 (12) for the PAO1 genome, available from *Pseudomonas.com*. We calculated the expected values for gene expression for each gene under an additive gene-expression model by summing the expression values for both signals when added in isolation. Both these expected values and the observed expression values when both signals were added were square root-transformed before analysis to homogenize variances. We fit the model with the following structure: observed values for the addition of both signals as a response variable; separate intercepts for both nonsecretome and secretome genes; and expected expression values under additive effects of the signals as an offset [model code: $\text{lm}(\text{sqrt}(\text{observed}) \sim \text{secretome} - 1, \text{offset} = \text{sqrt}(\text{expected}))$]. With this model formulation, an intercept significantly greater than zero indicates synergistic effects of the signals on gene expression, whereas an intercept of less than zero indicates interference between the signals (Table S1). The inclusion of whether or not a gene is in the secretome as a factor in the model was supported by an F test ($F_{2,262} = 14.18$, $P = 1.42 \times 10^{-6}$).

- Crespi BJ (2001) The evolution of social behavior in microorganisms. *Trends Ecol Evol* 16(4):178–183.
- West SA, Diggle SP, Buckling A, Gardner A, Griffin AS (2007) The social lives of microbes. *Annu Rev Ecol Syst* 38:53–77.
- Darch SE, West SA, Winzer K, Diggle SP (2012) Density-dependent fitness benefits in quorum-sensing bacterial populations. *Proc Natl Acad Sci USA* 109(21):8259–8263.
- Redfield RJ (2002) Is quorum sensing a side effect of diffusion sensing? *Trends Microbiol* 10(8):365–370.
- Hense BA, et al. (2007) Does efficiency sensing unify diffusion and quorum sensing? *Nat Rev Microbiol* 5(3):230–239.
- Platt TG, Fuqua C (2010) What's in a name? The semantics of quorum sensing. *Trends Microbiol* 18(9):383–387.
- West SA, Winzer K, Gardner A, Diggle SP (2012) Quorum sensing and the confusion about diffusion. *Trends Microbiol* 20(12):586–594.
- Schmid-Hempel P, Frank SA (2007) Pathogenesis, virulence, and infective dose. *PLoS Pathog* 3(10):1372–1373.
- Lin W, Kovacicova G, Skorupski K (2007) The quorum sensing regulator HapR downregulates the expression of the virulence gene transcription factor AphA in *Vibrio cholerae* by antagonizing Lrp- and VpsR-mediated activation. *Mol Microbiol* 64(4):953–967.
- Jadhav GP, et al. (2011) Immunosuppressive but non-LasR-inducing analogues of the *Pseudomonas aeruginosa* quorum-sensing molecule N-(3-oxododecanoyl)-L-homoserine lactone. *J Med Chem* 54(9):3348–3359.
- Beatson SA, Whitchurch CB, Sargent JL, Levesque RC, Mattick JS (2002) Differential regulation of twitching motility and elastase production by Vfr in *Pseudomonas aeruginosa*. *J Bacteriol* 184(13):3605–3613.
- Yu NY, et al. (2010) PSORTb 3.0: Improved protein subcellular localization prediction with refined localization subcategories and predictive capabilities for all prokaryotes. *Bioinformatics* 26(13):1608–1615.

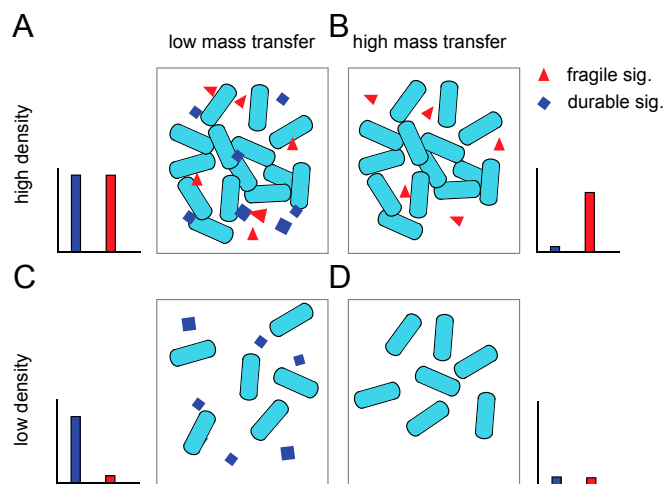


Fig. S1. Multiple signals allow simultaneous inferences on bacterial density and mass transfer regimes. The panels show schematically environments with high (A and B) and low (C and D) densities, along with high (B and D) and low (A and C) rates of mass transfer. The associated bar charts illustrate the “bacterial eye view” of resulting signal densities. With only one signal, there is not enough information to simultaneously resolve variations in density vs. variations in diffusion. However, with two appropriately parameterized signal molecules, each of the four basic environments (high/low density and high/low mass transfer) gives a distinct signal distribution signature.

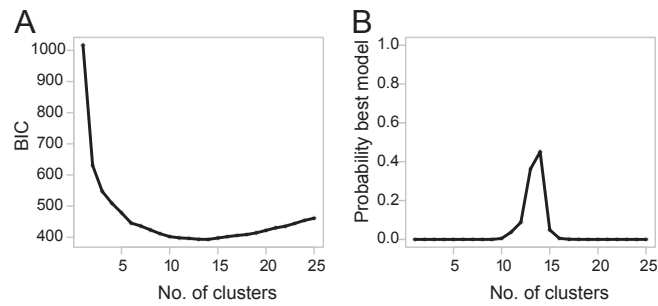


Fig. 56. The Bayesian information criterion (BIC) (A) and probability (B) of being the best model for differing cluster numbers for the expression-profile data. The data give most support for 14 clusters of expression profiles.

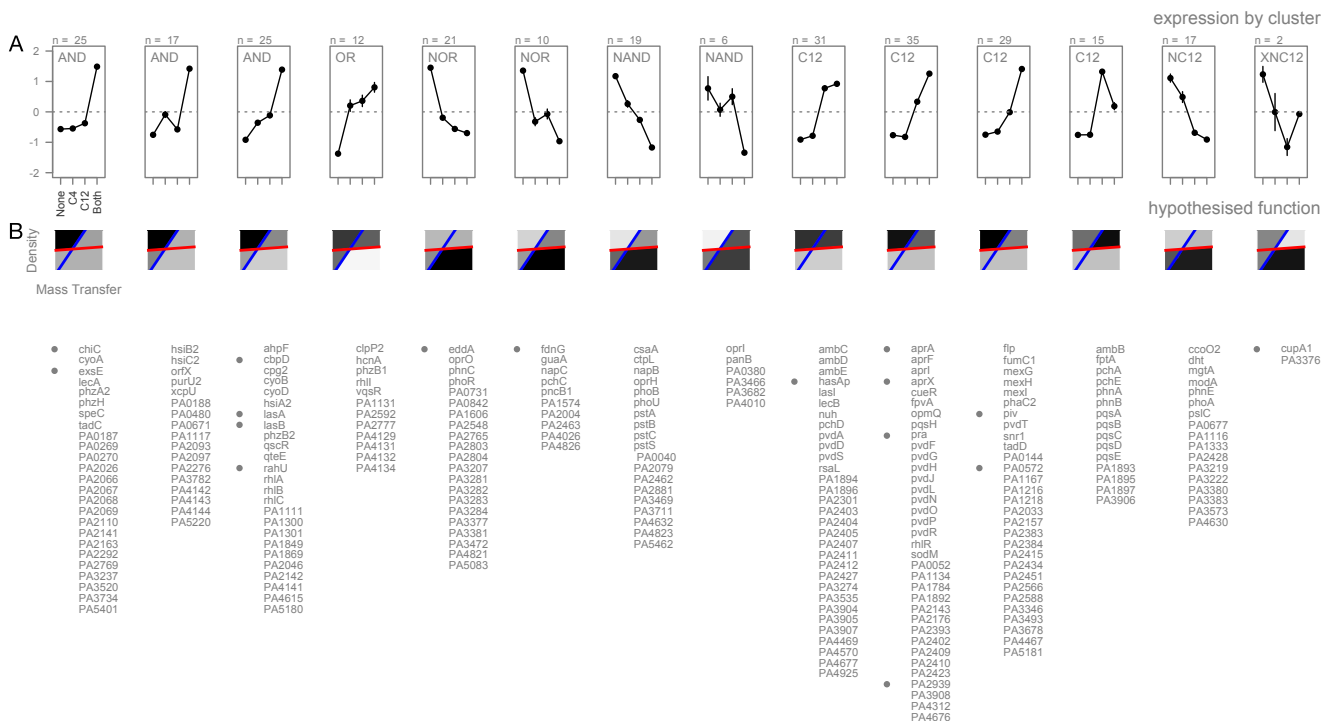


Table S2. Many quorum-sensing bacteria use multiple signals

Organism	Major signal molecules	Signal response genes	Signal synthase genes	QS-regulated phenotypes
<i>Burkholderia cenocepacia</i>	C6-HSL, C8-HSL	CepR, CciR	Cepl, Ccil	Exoenzymes, biofilm formation, swarming motility, siderophore, virulence
<i>Burkholderia pseudomallei</i>	C8-HSL, C10-HSL, 3-hydroxy-C8-HSL, 3-hydroxy-C10-HSL, 3-hydroxy-C14-HSL	PmlIR1, BpmR2, BpmR3	PmlI1, PmlI2, PmlI3	Virulence, exoprotease
<i>Burkholderia mallei</i>	C8-HSL, C10-HSL	BmaR1, BmaR3, BmaR4, BmaR5	Bmal1, Bmal3	Virulence
<i>Pseudomonas aeruginosa</i>	C4-HSL; C6-HSL, 3-oxo-C12-HSL	LasR, RhlR, QscR, VqsR	LasI, RhII	Exoenzymes, exotoxins, protein secretion, biofilms, swarming motility, secondary metabolites, 4-quinolone signaling, virulence
<i>Rhizobium leguminosarum</i> bv <i>viciae</i>	C14:1-HSL, C6-HSL, C7-HSL, C8-HSL, 3-oxo-C8-HSL, 3-hydroxy-C8-HSL	CinR, RhiR, RaiR, TraR, BisR, TriR	CinI, Rhil, Rail	Root nodulation/symbiosis, plasmid transfer, growth inhibition; stationary phase adaptation
<i>Yersinia pseudotuberculosis</i>	C6-HSL, 3-oxo-C6-HSL, C8-HSL	YpsR, YtbR	YpsI, YtbI	Motility, aggregation
<i>Vibrio harveyi</i>	3-hydroxy-C4-HSL, AI-2, CAI-1	LuxN, LuxPQ, CqsS	LuxM, LuxS, CqsS	Bioluminescence, biofilm production, type III secretion, protease production
<i>Vibrio fischeri</i>	3-oxo-C6-HSL, 3-oxo-C8-HSL	LuxR, AinR	LuxI, AinS	Bioluminescence, colonization
<i>Bacillus subtilis</i>	ComX, CSF	comX, antagonize the inhibitory activity of the Rap proteins on ComA	ComP/ComA	Sporulation, competence

Shown are several examples in well-studied bacteria. For each species shown, the major signal molecules, receptors, synthase genes, and types of genes that are QS-regulated in the system are listed (1–3).

1. Williams P, Winzer K, Chan WC, Cámara M (2007) Look who's talking: communication and quorum sensing in the bacterial world. *Philos Trans R Soc Lond B Biol Sci* 362(1483):1119–1134.
2. López D, Kolter R (2010) Extracellular signals that define distinct and coexisting cell fates in *Bacillus subtilis*. *FEMS Microbiol Rev* 34(2):134–149.
3. Schuster M, Sexton DJ, Diggle SP, Greenberg EP (2013) Acyl-homoserine lactone quorum sensing: from evolution to application. *Annu Rev Microbiol* 67:43–63.